JOURNAL OF GEOPHYSICAL RESEARCH, VOL. 114, A02302, doi:10.1029/2008JA013819, 2009

Seasonal variations of the ionospheric electron densities retrieved from Constellation Observing System for Meteorology, Ionosphere, and Climate mission radio occultation measurements

Libo Liu,[1] Biqiang Zhao,[1] Weixing Wan,[1] Baiqi Ning,[1] Man-Lian Zhang,[1] and Maosheng He[1]

Received 14 October 2008; revised 14 November 2008; accepted 2 December 2008; published 6 February 2009.

[1] We collected the ionospheric electron density (N_e) profiles from the FORMOSAT-3/COSMIC (F3/C) radio occultation measurements to investigate the seasonal behaviors of daytime N_e in the altitude range of 200–560 km. Harmonic analysis of the N_e at different altitudes provides unprecedented detail of the seasonal behaviors of N_e at low solar activity (LSA). Global maps of seasonal harmonic components indicate that there are strong annual and semiannual variations in daytime N_e, which have distinct latitudinal and altitudinal dependency. The semiannual component predominates over the annual variation in the equatorial regions and at high latitudes in the East Asian and South Atlantic sectors at low altitudes, and at higher altitudes the semiannual component predominates in the equatorial region, but recedes in other regions. The semiannual variation peaks in equinoctial months in most regions, while it has maxima in solstice months, first in the South Pacific region (around 30°S, 120°W) at 250 km altitude and expanding over the South Pacific and South Atlantic oceans at higher altitudes. Moreover, there is a region around 45°S, 30°W with a dominant semiannual component, moving toward east-north with increasing altitude in the range of 200–270 km. These two interesting features are novel but are not reported yet. The relative amplitude of the annual component of N_e has hemispheric asymmetry, which is prominent at high altitudes in the Southern Hemisphere. The winter/seasonal anomaly widely exists in the Northern Hemisphere and southern low latitudes and in Indian Ocean region at low altitudes but gradually disappears at higher altitudes. Further, in equatorial regions, a new finding is the obvious wave-like pattern in the longitudinal structure of the amplitudes of seasonal harmonic components in equatorial regions, which supports possible couplings of sources with lower atmospheric origins in the longitudinal variations of N_e.

Citation: Liu, L., B. Zhao, W. Wan, B. Ning, M.-L. Zhang, and M. He (2009), Seasonal variations of the ionospheric electron densities retrieved from Constellation Observing System for Meteorology, Ionosphere, and Climate mission radio occultation measurements, *J. Geophys. Res.*, *114*, A02302, doi:10.1029/2008JA013819.

1. Introduction

[2] It is well known that there are significant temporal and spatial variations in the Earth's ionospheric F layer. Among these variations, annual and semiannual variations are outstanding features of the F layer N_e variations. The characteristics of the seasonal variations of the F layer N_e depend on altitude, latitude, longitude, local time, and the phase of solar cycle. Although it has been studied for decades, the seasonal variation of the ionosphere is still one of the questions not fully solved [*Rishbeth*, 2004], partly due to the limitations of observation techniques and uneven data coverage. There is a need for more ionospheric measurements, particularly on the altitudinal structure and in oceanic regions, to provide not only a fuller understanding of the ionospheric seasonal features but also more accurate ionospheric models for related applications.

[3] According to the Chapman ionization theory, N_e in the ionosphere should behave in a way that is controlled by the solar zenith angle; that is, for the seasonal variation, N_e should be greater in summer than in equinox, and smallest in winter. However, previous studies have revealed some interesting "anomalous" features [e.g., *Bailey et al.*, 2000; *Balan et al.*, 1998, 2000; *Mendillo et al.*, 2005; *Richards*, 2001; *Rishbeth*, 1998; *Rishbeth et al.*, 2000; *Rüster and King*, 1973; *Su et al.*, 1998; *Torr and Torr*, 1973; *Torr et al.*, 1980; *Wright*, 1963; *Yonezawa*, 1971; *Zhang et al.*, 2005; *Zou et al.*, 2000], which are quite different from the prediction of the Chapman ionization theory. Historically, when the behaviors of the F_2 layer were significantly deviated from the solar zenith angle dependence as the

[1]Beijing National Observatory of Space Environment, Institute of Geology and Geophysics, Chinese Academy of Sciences, Beijing, China.

0148-0227/09/2008JA013819$09.00

Chapman ionization theory predicted, they were called "anomalies." Typical anomalies in the F_2 layer N_e are the so-called seasonal anomaly or winter anomaly (that the daytime values of midlatitude peak N_e of the F_2 layer, N_mF_2, are greater in winter than in summer), annual anomaly or nonseasonal anomaly (take the Northern and Southern hemispheres as a whole, N_mF_2 in December is greater than in June at both daytime and night), semiannual anomaly (greater N_mF_2 at equinox than at solstice), equatorial ionization anomaly (EIA, the equatorial anomaly is within approximately ±20° of the magnetic equator), and so on [e.g., *Ivanov-Kholodny and Mikhailov*, 1986; *Moffett*, 1979; *Torr and Torr*, 1973; *Torr et al.*, 1980]. The annual anomaly or nonseasonal anomaly is sometime called the annual asymmetry, which has been investigated using N_mF_2 [e.g., *Yonezawa*, 1971; *Rishbeth and Müller-Wodarg*, 2006; *Zeng et al.*, 2008], and the total electron content (TEC) from pair stations [e.g., *Titheridge and Buonsanto*, 1983] and networks of Global Positioning System (GPS) [*Mendillo et al.*, 2005; *Zhao et al.*, 2007] and other missions [*H. Liu et al.*, 2007]. Such anomalies are now explained in terms of the seasonal changes in atmospheric compositions and/or dynamic processes [e.g., *Bailey et al.*, 2000; *Mendillo et al.*, 2005; *Rishbeth*, 1998; *Rishbeth et al.*, 2000], which were unknown in Chapman's time. *Duncan* [1969] and *Rishbeth et al.* [2000] reviewed the various F region seasonal anomaly theories and restudied F region seasonal behavior.

[4] Since the discovery of the winter anomaly in daytime f_oF_2 (the critical frequency of the F_2 layer) by *Kirby et al.* [1934] and the semiannual effect in the F_2 region by O. Burkard in 1951, there are many studies on the ionospheric seasonal behaviors, conventionally conducted with f_oF_2 or N_mF_2, and TEC [e.g., *Feichter and Leitinger*, 1997; *Huang et al.*, 1989; *Jakowski et al.*, 1981; *Ma et al.*, 2003; *Mayr and Mahajan*, 1971; *McNamara and Smith*, 1982; *Torr and Torr*, 1973; *Unnikrishnan et al.*, 2002; *Yonezawa*, 1971; *Yu et al.*, 2004; *Yuen and Roelofs*, 1967; *Zeng et al.*, 2008; *Zou et al.*, 2000] as well as modelings [e.g., *Millward et al.*, 1996; *Pavlov and Pavlova*, 2005; *Richards*, 2001].

[5] For example, using f_oF_2 during 1958–1965 at various American stations, *Mayr and Mahajan* [1971] found that low-latitude N_mF_2 is larger in summer than in winter at low solar activity (LSA), while during high solar activity (HSA) the semiannual effect prevails at low latitudes and the winter anomaly prevails at midlatitudes. *Torr and Torr* [1973] constructed global maps of annual and semiannual variations for different levels of solar activity with f_oF_2 data from 140 stations. They reported that the winter/seasonal anomaly predominates at most locations and is more evident at HSA than at LSA. The differences in midlatitude N_mF_2 between the two solstices are stronger in the Northern Hemisphere than in the Southern Hemisphere. *Yu et al.* [2004] also reported the daytime seasonal pattern in HSA years by using global ionosonde data. *Richards* [2001] examined the midlatitude N_mF_2 data and found a semiannual variation with equinox maxima for all levels of solar activity, which are stronger in the Southern Hemisphere. Moreover, *Ma et al.* [2003] analyzed data from 30 ionosonde stations in three longitudinal sectors to examine the characteristics of the semiannual variation in N_mF_2. Their result indicates that the semiannual variation of N_mF_2 is mainly present at daytime.

[6] Many studies have also found strong seasonal variations in TEC at different locations [e.g., *Yuen and Roelofs*, 1967; *Jakowski et al.*, 1981; *McNamara and Smith*, 1982; *Huang et al.*, 1989; *Meza and Natali*, 2008]. *Feichter and Leitinger* [1997] reported that the semiannual component of TEC is well developed at HSA, while the annual component predominates at LSA during the whole day, except in the interval 1100–1300 LT. In contrast, *Unnikrishnan et al.* [2002] showed that over Palehua (19°N, 206°E) the annual component of TEC slightly exceeds the semiannual component, and the TEC exhibits opposite equinoctial asymmetries at HSA and LSA.

[7] The F region seasonal behaviors are also examined by using data from the incoherent scatter radar (ISR) measurements [e.g., *Balan et al.*, 1997, 1998, 2000; *Fukao et al.*, 1991; *Kawamura et al.*, 2002; *Oliver et al.*, 2008; *Zhang et al.*, 2005; *Zhang and Holt*, 2007]. For example, *Kawamura et al.* [2002] studied the seasonal behavior at LSA using the Shigaraki (35°N, 136°E) middle and upper atmosphere (MU) radar observations and the Sheffield University plasmasphere-ionosphere (SUPIM) model. Also based on the MU radar observations, *Balan et al.* [1997, 1998, 2000] have studied the altitude dependence of annual and semiannual variations of N_e and temperatures at HSA. They found that below the peak height of the F_2 layer (h_mF_2) the N_e was greater in September than in March, while above h_mF_2 the N_e was greater in March.

[8] Compared with those at h_mF_2, only a limited number of analyses have studied the climatological patterns in the topside ionosphere [e.g., *Bailey et al.*, 2000; *Su et al.*, 1998, 2005; *Zhao et al.*, 2005],. With the Hinotori satellite observations (February 1981 to June 1982), *Su et al.* [1998] found a strong annual anomaly in the low-latitude ionosphere at 600 km altitude, while *Bailey et al.* [2000] revealed the existence of an equinoctial asymmetry in the topside N_e. Contrary to N_mF_2, N_e at 600 km altitude is higher in the summer hemisphere than in the winter hemisphere. Similar strong seasonal variations were also found for N_e at 840 km altitude by *L. Liu et al.* [2007a] and *Zhao et al.* [2005] based on Defense Meteorological Satellite Program (DMSP) observations.

[9] During the past decades, several techniques, such as in situ satellite measurements, ground and topside ionosondes, and incoherent scatter radars (ISRs), have been used for probing the structure of the ionosphere. With accumulated dataset of N_mF_2/f_oF_2, TEC, and N_e, the overall picture of the F layer seasonal variation becomes more and more clear. Hitherto, however, we still do not have enough information on the altitudinal dependence of the seasonal variations of N_e on a global scale. *Balan et al.* [1997, 1998, 2000], *Kawamura et al.* [2002], and *Zhang et al.* [2005] have conducted excellent work on this issue; however, more data from different locations are clearly required to provide a global picture of the seasonal variations of N_e in the ionosphere, especially the altitudinal structure. With the development of the Global Navigation Satellite System, such as GPS, ionospheric radio occultation (IRO) observations on board low Earth-orbiting (LEO) satellites have become a powerful new technique to remotely sense the ionosphere with global-scale coverage. Some studies have shown promising IRO results in comparison with other measurements. The N_e profiles retrieved from IRO measure-

ments on board LEO satellites, such as FORMOSAT-3/COSMIC [*Lei et al.*, 2007; *Lin et al.*, 2007; *Schreiner et al.*, 2007], CHAMP [e.g., *H. Liu et al.*, 2007] and other missions, bring a potential data resource for understanding global ionospheric structures and their behavior.

[10] In this report, we collect the FORMOSAT-3/COSMIC (F3/C for short) IRO N_e profiles during the interval from DOY (day of year) 194, 2006, to DOY 279, 2008, which are archived at the University Corporation for Atmospheric Research (UCAR, United States) to investigate the global seasonal features of N_e. Approximately 1000–2600 occultation events were registered per day by F3/C. With the huge database of N_e profiles, we conduct a statistical analysis on the seasonal behavior of N_e. Our emphasis is on its latitudinal and longitudinal distribution, particularly the altitudinal structure. The most significant feature in our results is the presence of complicated global structures in the seasonal variations of N_e, which has an interesting altitudinal dependency not reported previously.

2. Data Source and Processing

[11] The F3/C (a Constellation Observing System for Meteorology, Ionosphere, and Climate mission of six microsatellites) was launched on 15 April 2006 into a circular low-Earth orbit with an altitude of 512 km and a 72° inclination. Initially the six satellites were close to each other, and now they are in orbits at around 800 km altitude and 30° separation in longitude between each satellite. Each F3/C microsatellite carries a GPS receiver to obtain atmospheric and ionospheric information through recording the phase and Doppler shifts of GPS signals. Electron densities of the ionosphere can be retrieved from the F3/C IRO measurements [e.g., *Lei et al.*, 2007; *Lin et al.*, 2007; *Schreiner et al.*, 2007]. The inversion of N_e profiles from IRO observations is based on several assumptions. Among these assumptions, the local spherical symmetry may be a strong one. Although several attempts have been conducted to avoid this assumption, there is no significant improvement in the accuracy of the retrieved profiles. The horizontal structures in some cases may significantly affect the retrieved profiles. Fortunately, preliminary validations of the IRO N_e observations showed good agreements with measurements of globally distributed ISRs and ionosondes [*Garcia-Fernandez et al.*, 2005; *Jakowski et al.*, 2002; *Lei et al.*, 2007; *Schreiner et al.*, 1999, 2007; *Tsai and Tsai*, 2004]. This indicates that the F3/C IRO observations provide an unprecedented three-dimensional N_e data source for ionospheric physics studies. The reader is referred to read *Lei et al.* [2007], *Lin et al.* [2007], and *Schreiner et al.* [2007] for detailed description on the F3/C mission and IRO N_e profile inversion technique and to *Liu et al.* [2008] for the data distribution. This database has attracted the interests of the community [e.g., *Lin et al.*, 2007; *Liu et al.*, 2008; *Zeng et al.*, 2008].

[12] We collect the F3/C N_e data from DOY 194, 2006, to DOY 279, 2008, to investigate the N_e seasonal variation in the altitudinal range of 200–560 km. During this period the solar 10.7 cm flux $F_{10.7}$ was low, and hence we will analyze the ionosphere behavior at LSA. Moreover, we assume that there is a linear solar cycle effect of N_e [see *L. Liu et al.*, 2006, 2007b] when we examine the seasonal behavior.

[13] The seasonal variations of N_e for a location at a fixed local time can be considered to be a superposition of the annual (A_{annual}) and semiannual ($A_{semiannual}$) components and the mean term (A_0) as

$$N_e = A_0 + A_{annual} + A_{semiannual} + \varepsilon. \quad (1)$$

Here

$$\begin{aligned} A_{annual} &= C_{12}\cos\frac{2\pi d}{365.25} + S_{12}\sin\frac{2\pi d}{365.25} \\ &= A_{12}\cos\frac{2\pi}{365.25}(d - \varphi_{12}) \\ A_{semiannual} &= C_6\cos\frac{4\pi d}{365.25} + S_6\sin\frac{4\pi d}{365.25} \\ &= A_6\cos\frac{4\pi}{365.25}(d - \varphi_6), \end{aligned}$$

where ε is the corresponding residual term; d is DOY, the day number which is counted as 1 on 1 January and 365(366) on 31 December. A_{annual} has a 12-month cycle with maxima at φ_{12} and amplitude A_{12}, and $A_{semiannual}$ has a 6-month cycle with maxima at φ_6 and amplitude A_6. We further expand A_0 and the coefficients C_{12}, S_{12}, C_6, and S_6 in the expressions of A_{annual} and $A_{semiannual}$ to take account of the solar cycle dependency as was done by *L. Liu et al.* [2007a]; that is, we assume there is a linear solar activity dependency of A_0, C_{12}, S_{12}, C_6, and S_6:

$$\begin{aligned} A_0 &= A_{00} + A_{01}F_{10.7p}, \\ C_{i(=12,6)} &= C_{i0} + C_{i1}F_{10.7p}, \\ S_{i(=12,6)} &= S_{i0} + S_{i1}F_{10.7p}. \end{aligned} \quad (2)$$

Here $F_{10.7p} = (F_{10.7} + F_{10.7A})/2$, $F_{10.7}$ is the solar 10.7-cm flux index, and $F_{10.7A}$ is the 81-day average of $F_{10.7}$ centered on the day specified. The reason why we choose $(F_{10.7} + F_{10.7A})/2$ as solar proxy can be found in the work of *L. Liu et al.* [2006, 2007b]. At a given solar activity level $F_{10.7p}$, the amplitude of the ith component is

$$\sqrt{(C_{i0} + C_{i1}F_{10.7p})^2 + (S_{i0} + S_{i1}F_{10.7p})^2},$$

and the phase of the ith component is

$$\operatorname{atan}\left(\frac{S_{i0} + S_{i1}F_{10.7p}}{C_{i0} + C_{i1}F_{10.7p}}\right).$$

Then the phases are presented in units of months when the maximum of N_e occurs. The results shown in the following are normalized to that $(F_{10.7} + F_{10.7A})/2 = 74$.

[14] After checking the data quality of IRO N_e profiles, we apply a five-point moving smooth to individual profiles and interpolate the data to regular altitude levels (200–560 km). To examine the seasonal variations of N_e at any altitude, we collect all data points at this altitude falling within a bin, which is centered at specified local time, latitude, longitude. A least squares fitting is applied to the data points collected in each bin to extract the mean A_0 as well as amplitudes (A_{12}, A_6) and phases (φ_{12}, φ_6) of the annual and semiannual components using equation (1). To

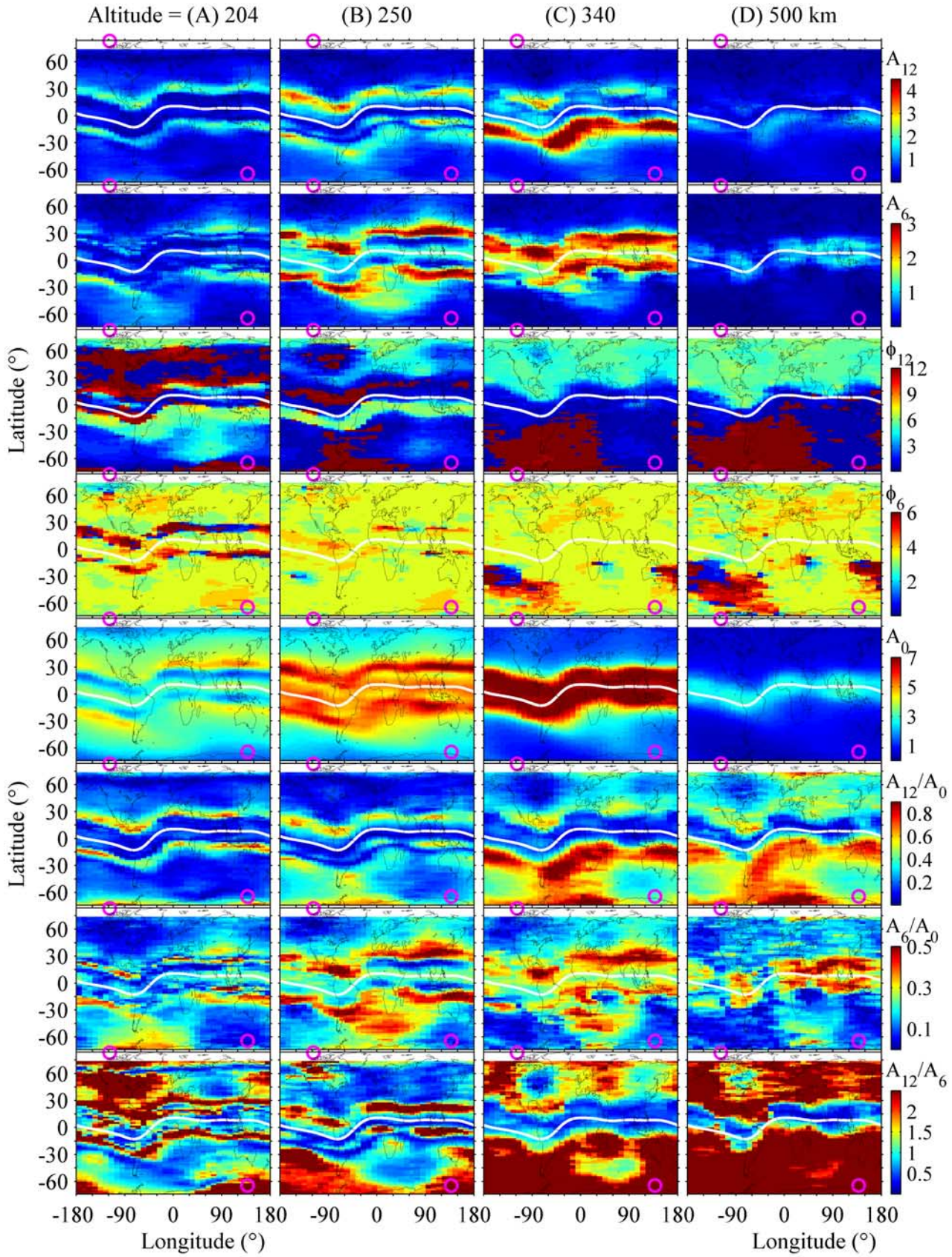
Altitude = (A) 204
(B) 250
(C) 340
(D) 500 km
A12
A6
ϕ12
ϕ6
A0
A12/A0
A6/A0
A12/A6
Latitude (°)
Longitude (°)
-180 -90 0 90 180
60 30 0 -30 -60

Figure 1

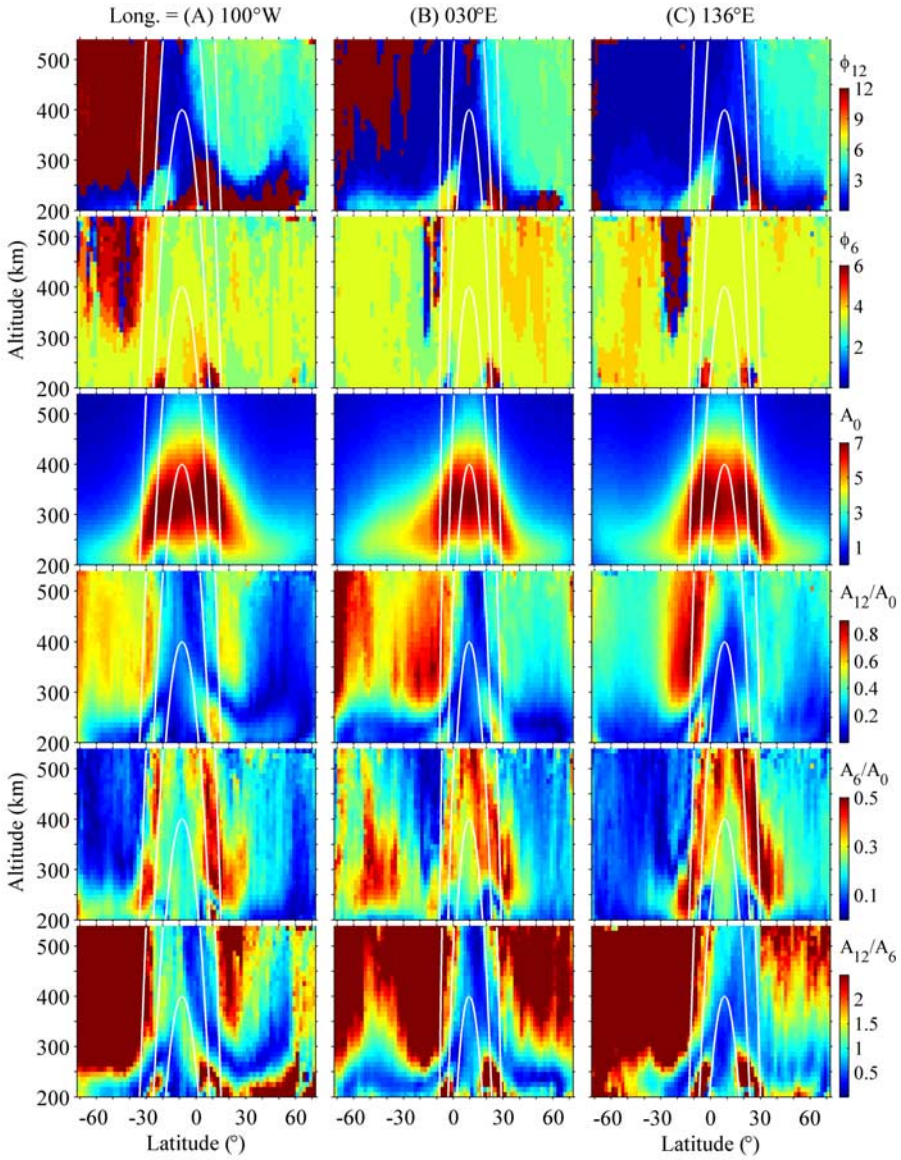

Figure 2. The altitudinal and geographic latitudinal variations of φ_{12}, φ_6, A_0, A_{12}/A_0, A_6/A_0, and A_{12}/A_6 of the F3/C N_e at geographic longitudes of (a) 100°W, (b) 30°E, and (c) 136°E at 1300 LT. In each panel the white curves indicate field lines. A_{12}, A_6, and A_0 are in units of 10^5 el/cm^3, and φ_{12} and φ_6 are in months.

provide ample points for a reliable fitting, the size of the cells was chosen to be 3 h in local time, 4° in latitude, and 30° in longitude.

3. Seasonal Variations of N_e

[15] Figure 1 shows global maps of A_{12}, A_6, φ_{12}, φ_6, A_0, A_{12}/A_0, A_6/A_0, and A_{12}/A_6 of N_e at altitudes of 204, 250, 340, and 500 km at 1300 LT. A_{12}, A_6, and A_0 of N_e are in units of 10^5 el/cm^3, and φ_{12} and φ_6 are in months. In each panel the white curve indicates the dip equator, and two magenta circles represent the locations of magnetic poles. To have a better understanding of the altitudinal dependence of global N_e seasonal behaviors, we plot in Figure 2 the φ_{12}, φ_6, A_0, A_{12}/A_0, A_6/A_0, and A_{12}/A_6 of N_e at 1300 LT as function of altitude and geographic latitude in three selected geographic longitude sectors (100°W, 30°E, and 136°E).

Figure 1. Maps of A_{12} (the amplitude of the annual component), A_6 (the amplitude of the semiannual component), φ_{12} (the phase of the annual component), φ_6 (the phase of the semiannual component), A_0 (annual mean), A_{12}/A_0, A_6/A_0, and A_{12}/A_6 of the F3/C N_e at altitudes of (a) 204, (b) 250, (c) 340, and (d) 500 km at 1300 LT. In each panel the white curve indicates the dip equator, and two magenta circles represent the locations of magnetic poles. A_{12}, A_6, and A_0 are in units of 10^5 el/cm^3, and φ_{12} and φ_6 are in months.

We also plot three geomagnetic field lines in white curves in each panel. Figure 1 illustrates the snapshots of the above parameters at given altitudes. From Figure 1 we can see the latitudinal and longitudinal structure of the seasonal variations of N_e. Figure 2 depicts results at selected longitudes, which gives us information on the altitudinal dependency and hemispheric differences. Combining Figure 1 and Figure 2, we can obtain a three-dimensional picture of the seasonal behavior of daytime N_e at low solar activity.

3.1. Relative Importance of Annual and Semiannual Components of N_e

[16] Take, for example, 204 km for low altitudes. As indicated by A_{12}/A_6 in the bottom left panel of Figure 1, the annual component of daytime N_e at low altitudes predominates over the semiannual component at northern midlatitudes and high latitudes in the near-pole regions. The pole here means magnetic pole (see magenta circles in each panel of Figure 1). The definition of near-pole and far-from-pole regions is similar to that of *Millward et al.* [1996], *Rishbeth* [1998], and *Zou et al.* [2000]. The near-pole regions refer to the North Atlantic sector and the Australasian sector in the Southern Hemisphere, and the East Asian and South Atlantic sectors are in the far-from-pole regions. A strong annual component is also present at two low-latitude bands, one in the Northern Hemisphere and another in the opposite hemisphere. It is interesting that these two bands are located at magnetic latitudes roughly parallel with the dip equator. In contrast, the semiannual component of N_e prevails at high latitudes in the far-from-pole regions as well as in the equatorial regions.

[17] Figure 1 also shows that an altitudinal transition exists in A_{12}/A_6 of N_e. At high altitudes the semiannual component of N_e still prevails in the equatorial regions and is significant at high latitudes in North America, while it gradually gives way to the annual component in other regions. It should be mentioned that the altitudinal transition of the relative importance of semiannual and annual components is quite complicated in the region around North America. As the bottom panels of Figure 1 illustrate, in this region the annual component is absolutely dominant at 204 km altitude. With the altitude increasing to 250 km the semiannual component becomes stronger. However, the annual component prevails again at 340 km altitude. In other words, the semiannual component is relatively more important than the annual one around the peak height at middle latitudes in the Northern Hemisphere, similar to the behavior of TEC in the North Atlantic region [*Meza and Natali*, 2008]. The situation in the Southern Hemisphere is much simpler; that is, with increasing altitude, the semiannual component gradually gives way to the annual component.

[18] The A_{12}/A_6 panels of Figure 1 and Figure 2 clearly show that the relative importance of the daytime annual and semiannual variations varies with altitude and latitude. In general, in the region between the two crests of the EIA, the values of N_e have obviously semiannual variations, which have a geomagnetic alignment along longitude [*Zou et al.*, 2000]. The contours tend to align with the dip equator (see Figure 1). There are two minima of A_{12}/A_6 in latitude at altitudes around 280 km, one near the dip equatorial region and the second one in far-from-geomagnetic-pole high-latitude region. At higher altitudes, the annual component is pronounced at most latitudes and the semiannual component is prominent only in the equatorial region.

3.2. Annual Variation of N_e

[19] As illustrated in the A_{12} and A_{12}/A_0 panels of Figure 1, at 204 km altitude, the low-latitude maxima are obvious in the absolute (A_{12}) and relative (A_{12}/A_0) amplitudes of the annual component. At altitudes of 340 km and 500 km a hemispheric asymmetry in the amplitude of the annual component becomes pronounced, with a stronger one at middle latitudes and in the far-from-pole regions in the Southern Hemisphere. Both A_{12} and A_{12}/A_0 in the 500 km altitude panel of Figure 1 are much stronger in the Southern Hemisphere than in the northern one. It can also be seen in the A_{12}/A_0 panel of Figure 2 that this hemispheric asymmetry in A_{12}/A_0 is distinct at altitudes above about 260 km. A striking aspect is the small altitudinal variation in A_{12}/A_0 at altitudes above 260 km. Meanwhile, there are two maxima of A_{12}/A_0 in the Southern Hemisphere, one at low latitude and one at high latitudes in the far-from-pole region. Further, a novel finding is that the wave-like pattern can be found in the longitudinal structure of A_0 and A_{12}/A_0 at low latitude. Four peaks are obviously presented in the results at 250 km.

[20] Concerning the annual phase, the annual variation at 204 km altitude peaks around December solstice in most regions in the Northern Hemisphere and the far-from-pole region in the Southern Hemisphere, whereas it peaks around March equinox to June solstice at low latitudes and in the near-pole region in Southern Hemisphere (see the φ_{12} panel of Figure 1); hence there is a winter/seasonal anomaly over most regions in the Northern Hemisphere and southern low latitudes at low altitudes. However, φ_{12} shows entirely different behaviors at high altitudes in both hemispheres. With increasing altitude, φ_{12} in the Northern Hemisphere shifts toward June solstice, first in far-from-pole regions, and gradually extends to the whole middle and low latitudes. Meanwhile, in the Southern Hemisphere φ_{12} also gradually shifts to local summer months. In other words, the annual component tends to have maxima in local summer months at higher altitudes. Consequently the winter/seasonal anomaly disappears at high altitudes in most regions.

[21] The top panels of Figure 2 depict the altitudinal variations of φ_{12} at different latitudes in three longitudes. In the Southern Hemisphere the annual component has maxima around December solstice at most altitudes. The φ_{12} shifts from January or equinoctial months (in the South Atlantic Ocean and Indian Ocean; see 30°E in Figure 2, for example) around 220–250 km to December solstice at high altitudes, and at low latitudes the shift in φ_{12} is from June solstice to December solstice. In contrast, in the Northern Hemisphere φ_{12} peaks around December solstice for altitudes below about 250–270 km, while it gradually peaks toward June solstice at higher altitudes. As a result, the values of N_e at high altitudes in summer exceed those in winter, which is quite consistent with previous investigations [e.g., *Su et al.*, 1998; *L. Liu et al.*, 2007a].

3.3. Semiannual Variation of N_e

[22] The A_6 and A_6/A_0 panels of Figure 1 show that at 204 km altitude the semiannual component of daytime N_e

has maxima at low latitudes in the Southern and Northern hemispheres. The bands of the maxima are marking the location of the EIA. Further, the semiannual component dominates in the far-from-pole regions in the Southern Hemisphere, which is in more detail in the A_{12}/A_6 panel of Figure 2 for the result at geographic longitude 30°E sector. Moreover, the low-latitude A_6 peaks around the crests of EIA, in parallel with the dip equator. Therefore *Ma et al.* [2003] suggested that the main cause of the semiannual variations is related to the ionospheric fountain effect. As illustrated in the A_6/A_0 panel of Figure 2, the maxima of A_6/A_0 of N_e at low latitudes have an arch structure, and its equatorial peak extends to a higher altitude compared with that of A_0. This latitudinal and altitudinal pattern suggests the control of geomagnetic field, indirectly depicting the important role of dynamic processes in the semiannual variation in the equatorial and low latitude regions.

[23] In addition, in the far-from-pole region the semiannual component is more pronounced in the altitudinal range of 250–450 km. If we take snapshots of A_6/A_0 at different altitudes (figures not shown here), we can see that as the altitude lifts, the location with dominant semiannual component moves in the direction toward east-north in the South Pacific Ocean region. This is also a novel phenomenon. This feature can also be found if we compare the A_6/A_0 results at 204 km and 250 km in Figure 1.

[24] As shown in the φ_6 panel of Figure 1, the semiannual component has maxima in equinoctial months in most regions over the global. The φ_6 maximum occurs in solstice months only in the low-latitude bands at low altitudes. With increasing altitude, this anomalous area in the equatorial region quickly recedes and is no longer discernable at 340 km. At higher altitudes, solstice maxima also occur at southern middle latitudes in the American sector. As illustrated in the φ_6 panel of Figure 1, the semiannual variation peaks in solstice months first around geographic 30°S, 120°W at 250 km altitude, and the area expands in latitude and longitude extending over the South Pacific and South Atlantic oceans at higher altitudes. The altitudinal evolution of this feature is more obvious in the φ_6 panels in Figure 2 for geographic longitude 100°W and 136°E. This interesting feature is also not reported yet in the literature.

3.4. Annual Mean of N_e

[25] Turning to the annual mean values of N_e, the A_0 panels of Figures 1 and 2 depict the well-known EIA structure in equatorial and low latitudes. There is a hump latitudinal structure in A_0. The EIA crests of A_0 are merged together into a single peak in the dip equatorial region at high altitudes. The low-latitude peaks in A_0 roughly align along with the dip equator.

[26] A new feature is that at low altitudes (below 240 km), two bands are found with depleted A_0 at the equatorial side of the low-latitude maxima straddling with higher values around the dip equator. The two bands with depleted A_0 at low altitudes exist in all longitudes. With increasing altitude, the feature disappears. From the A_0 panel in Figure 2, we note that there are two plasma caves with depressed A_0 around 200–230 km underlying the crests of EIA in both hemispheres. Therefore the two plasma caves in A_0 exist in all longitudes.

[27] Another finding is that a wave-like pattern is obviously present in the longitudinal structure of A_{12}, A_6, A_0, A_6/A_0, and A_{12}/A_6 in the equatorial region. It indicates the existence of a longitudinal wave-like structure in the seasonal variations of N_e, which is reported for the first time. The wave-like longitudinal pattern has been found in airglow observations [*Henderson et al.*, 2005; *Immel et al.*, 2006; *Sagawa et al.*, 2005] and daytime N_e [e.g., *Lin et al.*, 2007; *Lühr et al.*, 2007], TEC [*Wan et al.*, 2008], electron temperature [*Ren et al.*, 2008], and scale height [*Liu et al.*, 2008], etc. It has long been recognized that the tilt of the magnetic field configuration is the ultimate cause of the longitudinal dependence of ionospheric annual variation. However, recent works suggest possible couplings of sources with lower atmospheric origins, like the nonmigrating tide mode DE3 [e.g., *Henderson et al.*, 2005; *Immel et al.*, 2006; *Wan et al.*, 2008]. Our results shown here also support this possibility, because the wave-like longitudinal variation of the seasonal behavior of N_e cannot be explained solely with the control of the magnetic field configuration.

4. Seasonal Variation of N_mF_2 and h_mF_2

[28] Figure 3 shows the global distribution of the seasonal variations of N_mF_2 and h_mF_2 around 1300 LT. We may have a much detailed map of the seasonal characteristics, compared with that of *Torr and Torr* [1973] and even the most recent work of *Yu et al.* [2004].

[29] A_{12}/A_0 of N_mF_2 in the left-hand panels illustrates the hemispheric asymmetry in the annual change of daytime N_mF_2, generally stronger in the Southern Hemisphere. A strong annual component appears at low latitudes as well as at high latitudes in the Southern Hemisphere. The daytime N_mF_2 has maxima around December solstice in most regions, while in Europe, Central America, and Indian Ocean the annual maxima occur around March.

[30] A hemispheric asymmetry also exists in the semiannual amplitude of daytime N_mF_2, generally stronger in northern low latitudes and also at southern middle and high latitudes in the far-from-pole region. We may note a simple picture in the semiannual phase of N_mF_2, prevailing globally in equinoctial months. An exception can be seen in φ_6 (with solstice months) in the southern Pacific Ocean. In this region, anomalous φ_6 have also been found in that of high-altitude N_e (see the φ_6 panels in Figure 1), as mentioned in the previous section.

[31] As depicted by the left-hand panel of A_{12}/A_6 in Figure 3a, the annual components of N_mF_2 are dominant in the near-pole regions and at low latitudes in the Southern Hemisphere, while the semiannual variations of N_mF_2 are relatively stronger in other regions.

[32] Recently, with the TOPEX data at LSA, *Meza and Natali* [2008] reported that at middle latitudes the main component is semiannual in North Atlantic and annual in South Atlantic. It is interesting that their TEC feature is quite similar with that of N_mF_2 in middle Atlantic regions. Moreover, although the global distribution of the seasonal behavior of N_mF_2 depends on solar activity, our LSA results are roughly consistent with those of *Yu et al.* [2004]. *Yu et al.* [2004] collected ionosonde data at HSA and derived that the annual variation of N_mF_2 is most pronounced at magnetic latitudes of 40°–60° in both hemispheres, while a

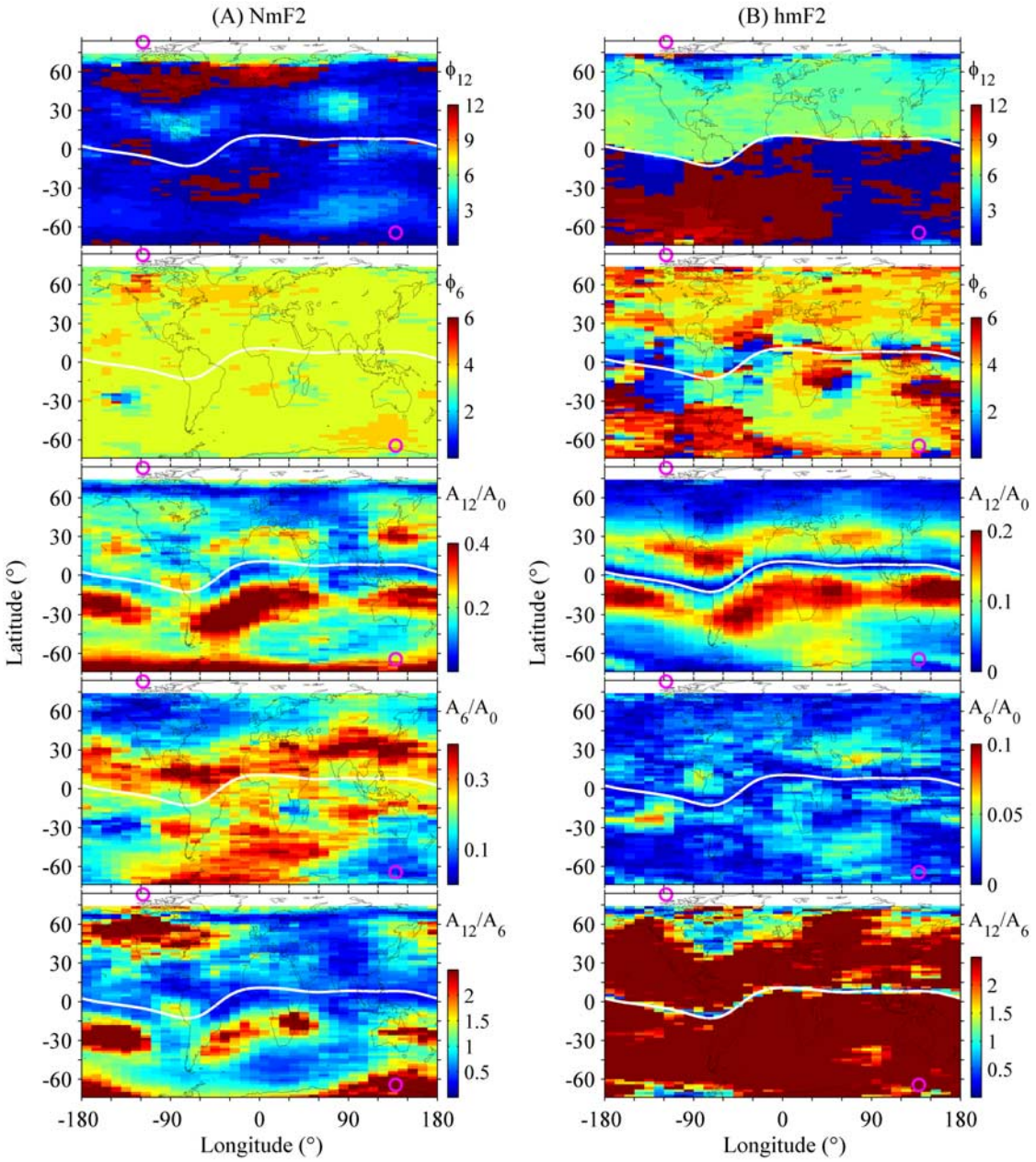

Figure 3. Global distribution of φ_{12}, φ_6, A_{12}/A_0, A_6/A_0, and A_{12}/A_6 of (a) N_mF_2 and (b) h_mF_2 at 1300 LT. The φ_{12} and φ_6 are in months. The white curve indicates the dip equator, and two magenta circles represent the locations of magnetic poles.

semiannual effect prevails in tropical regions and in the far-pole regions with maxima usually in March and April. Winter anomaly is most noticeable at high midlatitudes in the North American/European and Australian/Asian sectors at HSA. In other longitudes, and more generally in lower latitudes, the predominant variation of N_mF_2 is more or less semiannual, with maxima at or soon after the equinoxes. Of course, the region with winter anomaly is much smaller in our LSA results.

[33] Concerning h_mF_2, the annual component is dominant over the semiannual variation in most regions, which is distinctly depicted in the A_{12}/A_6 panel of Figure 3b. Semiannual variation becomes the main component at high latitudes in Northern America, mainly due to the smaller annual amplitude there.

[34] On the basis of ionosonde data, *Rishbeth et al.* [2000] revealed a semiannual component in low and middle latitude h_mF_2, which is comparable in amplitude to the annual variation. Their results are inconsistent with our results and also not reproduced by the thermosphere-ionosphere-mesosphere electrodynamics general circulation model (TIMEGCM) simulations. In contrast, the TIMEGCM simulations give a quite small semiannual component, which agrees with our result.

[35] The annual variation of h_mF_2 consistently peaks in June solstice in the Northern Hemisphere and around

December solstice in the Southern Hemisphere. As a result, daytime h_mF_2 is higher in summer than in winter, which is well known to us. What is striking for us is that the annual phase of h_mF_2 is well regulated by the sign of dip angle. This interesting feature reveals important information on the seasonal variations of dynamic processes, because h_mF_2 is strongly affected by dynamic processes, such as neutral winds and electric fields [e.g., *Oliver et al.*, 2008].

5. Discussion

[36] The basic physics and chemistry of the F_2 layer are thought to be well understood. The composition/solar zenith effects have implications for the ionosphere and can be used to explain the observed seasonal behaviors in the bottomside ionosphere. The seasonal variations of the ionosphere have been explained in terms of changes in solar zenith angle and thermospheric composition [e.g., *Rishbeth and Setty*, 1961; *Rüster and King*, 1973] and from global circulations [*Millward et al.*, 1996]. According to the generally accepted theory, the ionospheric N_e depends on the atomic/molecular ratio ($[O]/[N_2]$) as well as the solar zenith angle χ. Both observations and model simulations illustrate a clear seasonal change in thermospheric composition, specifically with higher $[O]/[N_2]$ in winter than in summer. *Rishbeth and Setty* [1961] first suggested the seasonal anomaly may be associated with atmospheric composition changes. There are much experimental and theoretical evidence of seasonal changes in the O/N_2 and O/O_2 ratios at thermospheric heights. The seasonal composition changes are induced by the prevailing summer-to-winter general circulations [e.g., *Duncan*, 1969]. The driving forces of this general circulation are heating due to solar radiation and energy from the solar wind deposited at high latitudes [e.g., *Millward et al.*, 1996; *Rishbeth*, 1998]. The high-latitude circulation is significantly geomagnetically controlled. There is a big offset of the magnetic pole from the geographic pole. Moreover, the importance of χ in seasonal variations of N_e is also quite different for different locations [*Millward et al.*, 1996]. As a result, the ionosphere in near-pole and far-from-pole regions shows different seasonal behaviors of N_e as illustrated in Figures 1 and 3. Detailed description is given by *Rishbeth* [1998], which has been used by *Yu et al.* [2004] and many other researchers to explain their N_mF_2 seasonal behaviors.

[37] Further, it has been known that several thermospheric parameters (such as neutral density, temperature, and compositions) vary semiannually, as has been known for decades. In terms of the offset of poles, *Millward et al.* [1996] have successfully simulated the observed semiannual effects at middle latitudes in the South American sector. Moreover, *Fuller-Rowell* [1998] suggested that the increased internal mixing at solstices can explain the semiannual neutral density variation and further that in N_mF_2. It is proposed that the global-scale circulation at solstice acts like a huge spoon to mix the major thermospheric species, causing less diffusive separation of the species at solstices. As a consequence, $[O]/[N_2]$ has clear annual and semiannual variations at most longitudes. The total mass density also has presented a clear semiannual variation [e.g., *Bowman et al.*, 2008; *H. Liu et al.*, 2005, 2007]. The semiannual variation of the ionosphere has ionization maxima in equinoxes and minima in solstices; the maxima arise from the optimized effect of the thermospheric composition and solar zenith angle at equinoxes when the thermospheric circulation is most symmetric.

[38] The semiannual variation in neutral density is a worldwide effect. There are no apparent latitude and altitude variations [*Bowman et al.*, 2008], which is also reproduced in empirical models (like the Mass Spectrometer Incoherent Scatter (MSIS). However, our analysis and other studies show strong altitudinal and latitudinal variations. Therefore finding the real source of the semiannual variation of N_e will be a challenging task.

[39] Besides the existence and relative importance of annual and semiannual variations, there is an altitudinal structure in the seasonal behaviors of N_e. Observational evidence indicates that the seasonal behavior in the topside ionosphere is rather different to that in the F region [e.g., *Balan et al.*, 2000; *Kawamura et al.*, 2002; *L. Liu et al.*, 2007a; *Su et al.*, 1998; *Zhao et al.*, 2005]. Our results in section 3 also clearly give us such a picture.

[40] It is well known that with increasing altitude, dynamics plays a more and more important role in the ionospheric evolution. Actually, the topside ionosphere is not in photochemical equilibrium and transport becomes one of the principal processes. Thus, besides neutral compositions, neutral winds should play an important role in the seasonal variations of N_e. Thermospheric winds push plasma up and down geomagnetic field lines and transport plasma from one hemisphere to the other by modulating the field-aligned flows, which influences the latitude structure of plasma [*Oyama and Watanabe*, 2004; *Watanabe et al.*, 1995] and the observed hemispheric asymmetries. Neutral winds in the magnetic meridian include contributions from both the geographic zonal and meridional winds, which depend on the magnetic declination angle. Therefore the field-aligned flows due to neutral winds may be a primary cause of the latitudinal and longitudinal dependences and the seasonal variations of the topside plasma densities [e.g., *Bailey et al.*, 2000; *Balan et al.*, 1997, 2000; *Su et al.*, 1998]. The seasonal variations of meridional winds may contribute to influence the seasonal variations of N_e, especially at which the thermospheric wind effects are particularly strong. Further, it is expected that the zonal wind also has contributions at longitudes with significant magnetic declinations [*Liu et al.*, 2004], giving the hemispheric asymmetries a longitudinal dependence (see Figure 3). As a result, the seasonal behavior exhibits altitudinal features because neutral winds play an important role in the high-altitude ionosphere. In terms of the effect of neutral wind, for example, *Balan et al.* [2000] proposed an explanation for the altitudinal variation of the seasonal behavior of N_e. Later, *Kawamura et al.* [2002] further extended this idea to explain the MU radar observations at LSA.

6. Summary

[41] We analyzed the N_e data from the F3/C IRO observations to investigate the global ionospheric seasonal behaviors at low solar activity. Harmonic analysis illustrates strong annual and semiannual components in the seasonal variations of N_e, which supports previous related studies and may stimulate a better understanding of the ionospheric

climatology. In summary, the major features are outlined as follows.

[42] 1. Electron densities at low altitudes (up to the F_2 layer peak) as well as N_mF_2 show a pronounced semiannual component in far-from-pole (high latitudes in the East Asian and South Atlantic sectors) and equatorial regions and strong annual variation in equatorial anomaly and near-pole regions. At high altitudes the semiannual variation still predominates in equatorial region but gives way to annual variation in other regions. In contrast, the annual component tends to have maxima in local summer months at higher altitudes, and consequently the winter/seasonal anomaly disappears at high altitudes in most regions.

[43] 2. A hemispheric asymmetry is found in the annual and semiannual amplitudes of N_mF_2 and high altitude N_e; the annual amplitude is more prominent at low and high latitudes in the Southern Hemisphere, and the semiannual one is stronger in the northern equatorial region and in the southern far-from-pole region.

[44] 3. The winter/seasonal anomaly widely exists at low altitudes but gradually disappears at high altitudes. In contrast, N_mF_2 has equinoctial maxima for the semiannual variation and December solstice peaks for the annual component in most regions, and the annual component prevails in daytime h_mF_2 in most regions with phase well regulated by the sign of dip angle.

[45] 4. Further, there are some interesting features not reported before. With increasing altitude, semiannual variation with solstice maxima expands over the South Pacific and South Atlantic oceans. An east-north movement is presented in the South Pacific region with dominant semiannual variation in the altitude ranges of 200 to 310 km. A wave-like pattern is obvious in the longitudinal structure of the amplitudes of seasonal harmonic components in equatorial regions similar to that observed earlier in N_mF_2.

[46] **Acknowledgments.** We greatly thank two reviewers for their detailed suggestions. This study made use of IRO data from the COSMIC Data Analysis and Archive Center (CDAAC). This research was supported by National Natural Science Foundation of China (40725014, 40674090, 40636032) and National Important Basic Research Project (2006CB806306).

[47] Wolfgang Baumjohann thanks Dieter Bilitza and Jan Lastovicka for their assistance in evaluating this paper.

References

Bailey, G. J., Y. Z. Su, and K.-I. Oyama (2000), Yearly variations in the low-latitude topside ionosphere, *Ann. Geophys.*, *18*, 789–798, doi:10.1007/s00585-000-0789-0.

Balan, N., Y. Otsuka, and S. Fukao (1997), New aspects in the annual variation of the ionosphere observed by the MU radar, *Geophys. Res. Lett.*, *24*, 2287–2290, doi:10.1029/97GL02184.

Balan, N., Y. Otsuka, G. J. Bailey, and S. Fukao (1998), Equinoctial asymmetries in the ionosphere and thermosphere observed by the MU radar, *J. Geophys. Res.*, *103*(A5), 9481–9495, doi:10.1029/97JA03137.

Balan, N., Y. Otsuka, S. Fukao, M. A. Abdu, and G. J. Bailey (2000), Annual variations of the ionosphere: A review based on MU radar observations, *Adv. Space Res.*, *25*(1), 153–162, doi:10.1016/S0273-1177(99)00913-8.

Bowman, B. R., W. K. Tobiska, and M. J. Kendra (2008), The thermospheric semiannual density response to solar EUV heating, *J. Atmos. Sol. Terr. Phys.*, *70*, 1482–1496, doi:10.1016/j.jastp.2008.04.020.

Duncan, R. A. (1969), F-region seasonal and magnetic storm behaviour, *J. Atmos. Terr. Phys.*, *31*, 59–70, doi:10.1016/0021-9169(69)90081-6.

Feichter, E., and R. Leitinger (1997), A 22-year cycle in the F layer ionization of the ionosphere, *Ann. Geophys.*, *15*, 1015–1027, doi:10.1007/s00585-997-1015-0.

Fukao, S., W. L. Oliver, Y. Onishi, T. Takami, T. Tsuda, M. Yamamoto, and S. Kato (1991), F-region seasonal behavior as measured by the MU radar, *J. Atmos. Terr. Phys.*, *53*, 599–618, doi:10.1016/0021-9169(91)90088-O.

Fuller-Rowell, T. J. (1998), The "thermospheric spoon": A mechanism for the semiannual density variation, *J. Geophys. Res.*, *103*, 3951–3956, doi:10.1029/97JA03335.

Garcia-Fernandez, M., A. Saito, J. M. Juan, and T. Tsuda (2005), Three-dimensional estimation of electron density over Japan using the GEONET GPS network combined with SAC-C data and ionosonde measurements, *J. Geophys. Res.*, *110*, A11304, doi:10.1029/2005JA011037.

Henderson, S. B., C. M. Swenson, A. B. Christensen, and L. J. Paxton (2005), Morphology of the equatorial anomaly and equatorial plasma bubbles using image subspace analysis of Global Ultraviolet Imager data, *J. Geophys. Res.*, *110*, A11306, doi:10.1029/2005JA011080.

Huang, Y.-N., K. Cheng, and S.-W. Chen (1989), On the equatorial anomaly of the ionospheric total electron content near the northern anomaly crest region, *J. Geophys. Res.*, *94*, 13,515–13,525, doi:10.1029/JA094iA10p13515.

Immel, T. J., E. Sagawa, S. L. England, S. B. Henderson, M. E. Hgan, S. B. Mende, H. U. Frey, C. M. Swenson, and L. J. Paxton (2006), Control of equatorial ionospheric morphology by atmospheric tides, *Geophys. Res. Lett.*, *33*, L15108, doi:10.1029/2006GL026161.

Ivanov-Kholodny, G. S., and A. V. Mikhailov (1986), *The Prediction of Ionospheric Conditions*, 167 pp., Springer, New York.

Jakowski, N., H. D. Bettac, B. Lazo, and L. Lois (1981), Seasonal variations of the columnar electron content of the ionosphere observed in Havana from July 1974 to April 1975, *J. Atmos. Terr. Phys.*, *43*, 7–11, doi:10.1016/0021-9169(81)90003-9.

Jakowski, N., A. Wehrenpfennig, S. Heise, C. Reigber, H. Lühr, L. Grunwaldt, and T. K. Meehan (2002), GPS radio occultation measurements of the ionosphere from CHAMP: Early results, *Geophys. Res. Lett.*, *29*(10), 1457, doi:10.1029/2001GL014364.

Kawamura, S., N. Balan, Y. Otsuka, and S. Fukao (2002), Annual and semiannual variations of the midlatitude ionosphere under low solar activity, *J. Geophys. Res.*, *107*(A8), 1166, doi:10.1029/2001JA000267.

Kirby, S. S., L. V. Berkner, and D. M. Stuart (1934), Studies of the ionosphere and their application to radio transmission, *Proc. Inst. Rad. Eng.*, *22*, 481–521.

Lei, J., et al. (2007), Comparison of COSMIC ionospheric measurements with ground-based observations and model predictions: Preliminary results, *J. Geophys. Res.*, *112*, A07308, doi:10.1029/2006JA012240.

Lin, C. H., C. C. Hsiao, J. Y. Liu, and C. H. Liu (2007), Longitudinal structure of the equatorial ionosphere: Time evolution of the four-peaked EIA structure, *J. Geophys. Res.*, *112*, A12305, doi:10.1029/2007JA012455.

Liu, H., H. Lühr, V. Henize, and W. Köhler (2005), Global distribution of the thermospheric total mass density derived from CHAMP, *J. Geophys. Res.*, *110*, A04301, doi:10.1029/2004JA010741.

Liu, H., H. Lühr, and S. Watanabe (2007), Climatology of equatorial thermospheric mass density anomaly, *J. Geophys. Res.*, *112*, A05305, doi:10.1029/2006JA012199.

Liu, L., X. Luan, W. Wan, J. Lei, and B. Ning (2004), Solar activity variations of equivalent winds derived from global ionosonde data, *J. Geophys. Res.*, *109*, A12305, doi:10.1029/2004JA010574.

Liu, L., W. Wan, B. Ning, O. M. Pirog, and V. I. Kurkin (2006), Solar activity variations of the ionospheric peak electron density, *J. Geophys. Res.*, *111*, A08304, doi:10.1029/2006JA011598.

Liu, L., B. Zhao, W. Wan, S. Venkartraman, M.-L. Zhang, and X. Yue (2007a), Yearly variations of global plasma densities in the topside ionosphere at middle and low latitudes, *J. Geophys. Res.*, *112*, A07303, doi:10.1029/2007JA012283.

Liu, L., W. Wan, X. Yue, B. Zhao, B. Ning, and M.-L. Zhang (2007b), The dependence of plasma density in the topside ionosphere on solar activity level, *Ann. Geophys.*, *25*(6), 1337–1343.

Liu, L., M. He, W. Wan, and M.-L. Zhang (2008), Topside ionospheric scale heights retrieved from Constellation Observing System for Meteorology, Ionosphere, and Climate radio occultation measurements, *J. Geophys. Res.*, *113*, A10304, doi:10.1029/2008JA013490.

Lühr, H., K. Häusler, and C. Stolle (2007), Longitudinal variation of *F* region electron density and thermospheric zonal wind caused by atmospheric tides, *Geophys. Res. Lett.*, *34*, L16102, doi:10.1029/2007GL030639.

Ma, R., J. Xu, and H. Liao (2003), The features and a possible mechanism of semiannual variation in the peak electron density of the low latitude F2 layer, *J. Atmos. Sol. Terr. Phys.*, *65*, 47–57, doi:10.1016/S1364-6826(02)00192-X.

Mayr, H. G., and K. K. Mahajan (1971), Seasonal variation in the F_2 region, *J. Geophys. Res.*, *76*, 1017–1027, doi:10.1029/JA076i004p01017.

McNamara, L. F., and D. H. Smith (1982), Total electron content of the ionosphere at 31°S, 1967–1974, *J. Atmos. Terr. Phys.*, *44*, 227–239, doi:10.1016/0021-9169(82)90028-9.

Mendillo, M., C. Huang, X. Pi, H. Rishbeth, and R. Meier (2005), The global ionospheric asymmetry in total electron content, *J. Atmos. Sol. Terr. Phys.*, *67*, 1377–1387, doi:10.1016/j.jastp.2005.06.021.

Meza, A., and M. P. Natali (2008), Annual and semiannual TEC effects at low solar activity in midlatitude Atlantic region based on TOPEX, *J. Geophys. Res.*, *113*, D14115, doi:10.1029/2007JD009088.

Millward, G. H., R. J. Moffett, S. Quegan, and T. J. Fuller-Rowell (1996), Ionospheric F_2 layer seasonal and semiannual variations, *J. Geophys. Res.*, *101*, 5149–5156, doi:10.1029/95JA03343.

Moffett, R. J. (1979), The equatorial anomaly in the electron distribution of the terrestrial F-region, *Fundam. Cosmic Phys.*, *4*, 313–391.

Oliver, W. L., S. Kawamura, and S. Fukao (2008), The causes of the midlatitude *F* layer behavior, *J. Geophys. Res.*, *113*, A08310, doi:10.1029/2007JA012590.

Oyama, K., and S. Watanabe (2004), Effects of zonal and meridional neutral winds on the electron density and temperature at the height of 600 km, JAXA research and development report, 12 pp., Jpn Aerosp. Explor. Agency.

Pavlov, A. V., and N. M. Pavlova (2005), Causes of the mid-latitude NmF2 winter anomaly, *J. Atmos. Sol. Terr. Phys.*, *67*, 862–877, doi:10.1016/j.jastp.2005.02.009.

Ren, Z., W. Wan, L. Liu, B. Zhao, Y. Wei, X. Yue, and R. A. Heelis (2008), Longitudinal variations of electron temperature and total ion density in the sunset equatorial topside ionosphere, *Geophys. Res. Lett.*, *35*, L05108, doi:10.1029/2007GL032998.

Richards, P. G. (2001), Seasonal and solar cycle variations of the ionospheric peak electron density: Comparison of measurement and models, *J. Geophys. Res.*, *106*(A12), 12,803–12,819, doi:10.1029/2000JA000365.

Rishbeth, H. (1998), How the thermospheric circulation affects the ionosphere, *J. Atmos. Sol. Terr. Phys.*, *60*, 1385–1402, doi:10.1016/S1364-6826(98)00062-5.

Rishbeth, H. (2004), Questions of the equatorial F2-layer and thermosphere, *J. Atmos. Sol. Terr. Phys.*, *66*, 1669–1674, doi:10.1016/j.jastp.2004.07.008.

Rishbeth, H., and I. C. F. Müller-Wodarg (2006), Why is there more ionosphere in January than in July? The annual asymmetry in the F2-layer, *Ann. Geophys.*, *24*, 3293–3311.

Rishbeth, H., and C. S. G. K. Setty (1961), The F-layer at sunrise, *J. Atmos. Terr. Phys.*, *21*, 263–276, doi:10.1016/0021-9169(61)90205-7.

Rishbeth, H., I. C. F. Müller-Wodarg, L. Zou, T. J. Fuller-Rowell, G. H. Millward, R. J. Moffett, D. W. Idenden, and A. D. Aylward (2000), Annual and semiannual variations in the ionospheric F2-layer: II. Physical discussion, *Ann. Geophys.*, *18*, 945–956, doi:10.1007/s00585-000-0945-6.

Rüster, R., and J. W. King (1973), Atmospheric composition changes and the F2-layer seasonal anomaly, *J. Atmos. Terr. Phys.*, *35*, 1317–1322, doi:10.1016/0021-9169(73)90164-5.

Sagawa, E., T. J. Immel, H. U. Frey, and S. B. Mende (2005), Longitudinal structure of equatorial anomaly in the nighttime ionosphere observed by IMAGE/FUV, *J. Geophys. Res.*, *110*, A11302, doi:10.1029/2004JA010848.

Schreiner, W., S. Sokolovskiy, C. Rocken, and D. Hunt (1999), Analysis and validation of GPS/MET radio occultation data in the ionosphere, *Radio Sci.*, *34*, 949–966, doi:10.1029/1999RS900034.

Schreiner, W., C. Rocken, S. Sokolovskiy, S. Syndergaard, and D. Hunt (2007), Estimates of the precision of GPS radio occulations from the COSMIC/FORMOSAT-3 mission, *Geophys. Res. Lett.*, *34*, L04808, doi:10.1029/2006GL027557.

Su, S.-Y., C. K. Chao, H. C. Yeh, and R. A. Heelis (2005), Seasonal and latitudinal distributions of the dominant light ions at 600 km topside ionosphere from 1999 to 2002, *J. Geophys. Res.*, *110*, A01302, doi:10.1029/2004JA010564.

Su, Y. Z., G. J. Bailey, and K.-I. Oyama (1998), Annual and seasonal variations in the low-latitude topside ionosphere, *Ann. Geophys.*, *16*, 974–985, doi:10.1007/s00585-998-0974-0.

Titheridge, J. E., and M. J. Buonsanto (1983), Annual variations in the electron content and height of the F layer in the northern and southern hemispheres, related to neutral compositions, *J. Atmos. Terr. Phys.*, *45*, 683–696, doi:10.1016/S0021-9169(83)80027-0.

Torr, D. G., M. R. Torr, and P. G. Richards (1980), Causes of the *F* region winter anomaly, *Geophys. Res. Lett.*, *7*, 301–304, doi:10.1029/GL007i005p00301.

Torr, M. R., and D. G. Torr (1973), The seasonal behaviour of the F2-layer of the ionosphere, *J. Atmos. Terr. Phys.*, *35*, 2237–2251, doi:10.1016/0021-9169(73)90140-2.

Tsai, L.-C., and W.-H. Tsai (2004), Improvement of GPS/MET ionospheric profiling and validation using Chung-Li ionosonde measurements and the IRI model, *Terr. Atmos. Oceanic Sci.*, *15*, 589–607.

Unnikrishnan, K., R. B. Nair, and C. Venugopal (2002), Harmonic analysis and an empirical model for TEC over Palehua, *J. Atmos. Sol. Terr. Phys.*, *64*, 1833–1840, doi:10.1016/S1364-6826(02)00187-6.

Wan, W., L. Liu, X. Pi, M. Zhang, B. Ning, J. Xiong, and F. Ding (2008), Wavenumber-4 patterns of the total electron content over the low-latitude ionosphere, *Geophys. Res. Lett.*, *35*, L12104, doi:10.1029/2008GL033755.

Watanabe, S., K.-I. Oyama, and M. A. Abdu (1995), Computer simulation of electron and ion densities and temperatures in the equatorial *F* region and comparison with Hinotori results, *J. Geophys. Res.*, *100*(A8), 14,581–14,590, doi:10.1029/95JA01356.

Wright, J. W. (1963), The *F* region seasonal anomaly, *J. Geophys. Res.*, *68*, 4379–4381.

Yonezawa, T. (1971), The solar-activity and latitudinal characteristics of the seasonal, non-seasonal and semi-annual variations in the peak electron densities of the F2-layer at noon and midnight in middle and low latitudes, *J. Atmos. Terr. Phys.*, *33*, 889–907, doi:10.1016/0021-9169(71)90089-4.

Yu, T., W. Wan, L. Liu, and B. Zhao (2004), Global scale annual and semi-annual variations of daytime NmF2 in the high solar activity years, *J. Atmos. Sol. Terr. Phys.*, *66*, 1691–1701, doi:10.1016/j.jastp.2003.09.018.

Yuen, P. C., and T. H. Roelofs (1967), Seasonal variations in ionospheric total electron content, *J. Atmos. Terr. Phys.*, *29*, 321–326, doi:10.1016/0021-9169(67)90203-6.

Zeng, Z., A. Burns, W. Wang, J. Lei, S. Solomon, S. Syndergaard, L. Qian, and Y. Kuo (2008), Ionospheric annual asymmetry observed by the COSMIC radio occultation measurements and simulated by the TIEGCM, *J. Geophys. Res.*, *113*, A07305, doi:10.1029/2007JA012897.

Zhang, S.-R., and J. M. Holt (2007), Ionospheric climatology and variability from long-term and multiple incoherent scatter radar observations: Climatology in eastern American sector, *J. Geophys. Res.*, *112*, A06328, doi:10.1029/2006JA012206.

Zhang, S.-R., J. M. Holt, A. P. van Eyken, M. McCready, C. Amory-Mazaudier, S. Fukao, and M. Sulzer (2005), Ionospheric local model and climatology from long-term databases of multiple incoherent scatter radars, *Geophys. Res. Lett.*, *32*, L20102, doi:10.1029/2005GL023603.

Zhao, B., W. Wan, L. Liu, X. Yue, and S. Venkatramn (2005), Statistical characteristics of the total ion density in the topside ionosphere during the period 1996–2004 using empirical orthogonal function (EOF) analysis, *Ann. Geophys.*, *23*, 3615–3631.

Zhao, B., W. Wan, L. Liu, T. Mao, Z. Ren, M. Wang, and A. B. Christensen (2007), Features of annual and semiannual variations derived from the global ionospheric maps of total electron content, *Ann. Geophys.*, *25*, 2513–2527.

Zou, L., H. Rishbeth, I. C. F. Muller-Wodarg, A. D. Aylward, G. H. Millward, T. J. Fuller-Rowell, D. W. Idenden, and R. J. Moffett (2000), Annual and semiannual variations in the ionospheric F2-layer: I. Modelling, *Ann. Geophys.*, *18*, 927–944, doi:10.1007/s00585-000-0927-8.

M. He, L. Liu, B. Ning, W. Wan, M.-L. Zhang, and B. Zhao, Beijing National Observatory of Space Environment, Institute of Geology and Geophysics, Chinese Academy of Sciences, Beijing 100029, China. (liul@mail.iggcas.ac.cn)